 FDMP, vol.1, no.2, pp.97-107, 2005

A Computational Study of Bubble Motion in Newtonian and Viscoelastic Fluids

Edwin Jiménez[1], Mark Sussman[2], and Mitsuhiro Ohta[3]

Abstract: The aim of this paper is to utilize a numerical model to compute bubble motion in quiescent Newtonian and viscoelastic liquids. For our numerical method, we use a coupled level set and volume-of-fluid method with a second order treatment for the jump conditions related to surface tension. We investigate axisymmetric gas-liquid systems with large density and viscosity ratios as well as buoyancy-driven flows with complex changes in topology. We present comparisons to previous computational results as well as experimental results.

keyword: Level set, Volume-of-fluid, Viscoelastic, Projection method, Adaptive mesh refinement

1 Introduction

The objective of this work is to compute bubble motion in Newtonian and viscoelastic fluids. Although there is an extensive number of numerical results concerning bubble motion in incompressible Newtonian fluids (Rudman (1998); Sussman and Smereka (1997); Ohta, Imura, Yoshida, and Sussman (2005); Kang, Fedkiw, and Liu (2000); Unverdi and Tryggvason (1992); Brackbill, Kothe, and Zemach (1992); Esmaeeli (2005)), the literature regarding computation of non-Newtonian bubble motion, in particular viscoelastic flow, is limited in comparison. Previous work regarding multiphase viscoelastic flows include the work of Noh, Kang, and Leal (1993) using a body fitted formulation, Pillapakkam and Singh (2001) using the level set method and Goktekin, Bargteil, and O'Brien (2004) also using the level set method. We remark that the work by Noh, Kang, and Leal (1993) is not suitable for large interfacial deformations. The work by both Pillapakkam and Singh (2001) and Goktekin, Bargteil, and O'Brien (2004) are suitable for large deformations, and so our work can be seen as an extension of their methods. The main distinction between our work and previous work using the level set method is our second order treatment of the jump conditions where surface tension is concerned (Sussman (2003); Sussman, Hussaini, Smith, Zhi-Wei, and Mihalef (2004)). A second order treatment allows one to compute on a coarse mesh where otherwise a fine mesh is required.

Bubble phenomena have important applications in industry such as underwater explosions, ink-jet devices, chemical separators, nuclear power plants, bioreactors, and combustion engines (see Ohta, Imura, Yoshida, and Sussman (2005) and references therein). Air bubbles in water have even been observed to have applications in nature; whales and dolphins employ a "bubble fence" to round up their prey (Marten, Shariff, Psarakos, and White (1996)).

In the manufacturing process of certain materials, the behavior of materials while in their fluid state can impact the resulting product. Example applications, including the study of "sharkskin" instability in extrusion processes, have been researched by Bechtel, Forest, Wang, and Zhou (1998); Migler, Son, Qiao, and Flynn (2002); Venet and Vergnes (2000); Nithi-Uthai and Manas-Zloczower (2003); Jansseune, Mewis, Moldenaers, Minale, and Maffettone (2000). With a numerical method, one can systematically analyze the stability of non-newtonian flows in relation to various physical properties such as surface tension, viscosity, density, and concentration of viscoelastic material. A numerical method also allows one to measure the viscoelastic stress anywhere in the flow field. Finally, while we focus on the Chilcott-Rallison model in this paper, we can replace our constitutive law with the constitutive law for any "complex" fluid such as for liquid crystal polymers (Bechtel, Forest, Wang, and Zhou (1998)).

Here, we will consider the two-dimensional axisymmetric problem of a gas bubble rising first in a Newtonian liquid and then in a viscoelastic liquid. We examine the steady state bubble shape in each fluid. In another study, we initialize the gas-liquid system with a gas bubble just below the free surface of the liquid, surface tension ef-

[1] Florida State University, Dept. of Math, Tallahassee, FL, USA.
[2] Florida State University, Dept. of Math, Tallahassee, FL, USA.
[3] Muroran Institute of Technology, Dept. of Applied Chemistry, Muroran, Hokkaido, Japan

fects dominate the flow dynamics, ultimately resulting in a liquid jet. As expected, the liquid jet exhibits characteristics unique to the type of fluid used.

Because of important industrial applications, such as in microscale jetting devices, similar liquid jet problems have already been investigated (Sussman and Puckett (2000)). However, liquids employed in ink-jet devices need not be Newtonian liquids. Therefore an accurate numerical description of bubble and jet phenomena for viscoelastic fluids can result in more realistic simulations.

It should be noted that in our simulations, the bubbles are initially set at an 'intermediate' stage, i.e., we do not consider bubble formation nor initial bubble conditions. We simply begin with a spherical bubble, for example, and evolve its motion according to the relevant governing equations. In a related note, a recent study by Ohta, Imura, Yoshida, and Sussman (2005) considers the effects of initial bubble conditions on the motion of a rising gas bubble.

Our numerical approach is a coupled level set and volume-of-fluid method (CLSVOF) (Sussman and Smereka (1997); Sussman and Puckett (2000); Sussman (2003)). In the level set method (LS), a smooth *level set function* ϕ is used to implicitly represent the interface between the gas and the liquid. Although there are many possible level set functions that can be used (for a good introduction to level set methods see, e.g., Sethian (1999)), typically ϕ is chosen to be a distance function, i.e., $\phi = -d$ in the gas and $\phi = d$ in the liquid, where $d = d(t)$ is the shortest distance from a point (r,z) to the free surface at time t. Denote the gas and liquid (or 'solvent') domain by Ω_G and Ω_S, respectively. Thus,

$$\begin{cases} \phi > 0 & \text{if } \phi \in \Omega_S \\ \phi < 0 & \text{if } \phi \in \Omega_G. \end{cases}$$

The interface between the liquid and gas is contained implicitly in the level set $\phi = 0$. For a detailed account on level set methods see Sethian (1999); Sussman and Smereka (1997); Sussman, Smereka, and Osher (1994).

The level set equation,

$$\phi_t + \mathbf{u}\cdot\nabla\phi = 0, \tag{1}$$

prescribes that the interface is advected along particle paths; $\mathbf{u}$ is the underlying velocity field obtained from the momentum equations. Due to discretization error, and in spite of the fact that $\mathbf{u}$ is a volume conserving velocity field, one might experience mass loss when discretely solving (1). To overcome this difficulty, we solve an additional equation for the volume of fluid function F,

$$F_t + \mathbf{u}\cdot\nabla F = 0, \tag{2}$$

where $F = 1$ in a computational cell containing only liquid, $F = 0$ in a computational cell containing only gas, and $0 < F < 1$ otherwise.

As contrasted from the level set equation (1), one can incorporate mass-conserving discretization schemes for solving (2). Since $\nabla\cdot\mathbf{u} = 0$, we can rewrite (2) as

$$F_t + \nabla\cdot(\mathbf{u}F) = 0, \tag{3}$$

and then discretize (3) in conservation form (see section 3.1). We remark that we can rewrite the level set equation (1) in conservation form as well, but since the level set function ϕ does not have a physical relation to "mass", solving (1) in conservation form will not guarantee mass conservation.

So, in our formulation we couple the level set method to the volume-of-fluid method. The slopes in the volume-of-fluid reconstruction step are taken from the level set function. The level set function, on the other hand, is taken to be the signed distance from the volume-of-fluid reconstructed interface. Details and validation of our coupled levelset and volume-of-fluid approach are given by Sussman and Puckett (2000); Sussman (2003).

2 Governing Equations

In this paper we use the viscoelastic model proposed by Chilcott and Rallison (1988); i.e. the FENE-CL dumbbell model. We can write the governing equations of motions for incompressible two-phase non-Newtonian flow, with surface tension written as a body force (Sussman and Puckett (2000)), as follows

$$\mathbf{u}_t + (\mathbf{u}\cdot\nabla)\mathbf{u} = \frac{1}{\rho(\phi)}\nabla\cdot\mathbf{T} - \frac{\sigma\kappa}{\rho(\phi)}\nabla H(\phi) + \mathbf{g} \tag{4}$$

$$\mathbf{T} = -p\mathbf{I} + 2\tilde{\eta}_S\mathbf{D} + \frac{\tilde{\eta}_P(\phi)}{\lambda}f(R)\mathbf{A} \tag{5}$$

$$\nabla\cdot\mathbf{u} = 0, \tag{6}$$

where the *polymer configuration tensor* $\mathbf{A}$ is the dyadic product of the dumbbell end-to-end vector $\mathbf{R}$, i.e., $\mathbf{A} =$

$\langle \mathbf{RR} \rangle$, λ is a characteristic *relaxation time*, and $\mathbf{T}$ is the *total stress tensor*. In the liquid, $\mathbf{A}$ satisfies

$$\mathbf{A}_t + \mathbf{u}\cdot\nabla\mathbf{A} = \mathbf{A}\cdot\nabla\mathbf{u} + \nabla\mathbf{u}^T\cdot\mathbf{A} - \frac{f(R)}{\lambda}(\mathbf{A}-\mathbf{I}) \tag{7}$$

where the function

$$f(R) = \frac{1}{1-R^2/L^2} = \frac{1}{1-\mathrm{tr}(\mathbf{A})/L^2}. \tag{8}$$

represents the nonlinear spring characteristics of the viscoelastic fluid. Here L is the maximum length of a polymer molecule relative to the equilibrium radius of gyration. $\mathbf{D}$ is the *rate of deformation tensor* defined by

$$\mathbf{D} = \frac{\nabla\mathbf{u} + \nabla\mathbf{u}^T}{2}.$$

Here ρ is the density, η_S is the solvent viscosity, $\eta_P = c\eta_S$ is the polymer viscosity, κ is the curvature, σ is the surface tension,

$$\tilde{\eta}_P = \begin{cases} \eta_P & \text{if } \phi > 0 \\ 0 & \text{if } \phi < 0, \end{cases}$$

and H is the Heaviside function defined by

$$H(\phi) = \begin{cases} 1 & \text{if } \phi \geq 0 \\ 0 & \text{if } \phi < 0. \end{cases} \tag{9}$$

Let us denote the density and viscosity in the solvent as ρ_S and η_S, respectively (and similarly for the gas). Then, using the Heaviside function, we can write the density and viscosity in the liquid and gas as

$$\begin{aligned} \rho(\phi) &= \rho_G(1-H(\phi)) + \rho_S H(\phi) \\ \tilde{\eta}_S(\phi) &= \eta_G(1-H(\phi)) + \eta_S H(\phi). \end{aligned}$$

The governing equations for interface motion are given by

$$F_t + \mathbf{u}\cdot\nabla F = 0$$

and

$$\phi_t + \mathbf{u}\cdot\nabla\phi = 0.$$

3 Numerical Algorithm

3.1 Advancing the Interface

As mentioned in the Introduction, a coupled level set and volume-of-fluid method (CLSVOF) is used to represent the free surface. We simultaneously solve the level set equation and the volume-of-fluid equation

$$\begin{aligned} &\phi_t + \mathbf{u}\cdot\nabla\phi = 0 \\ &F_t + \mathbf{u}\cdot\nabla F = 0. \end{aligned}$$

Define a typical computational cell to be

$$\Omega_{ij} = \{(x,y) | x_i \leq x \leq x_{i+1},\ y_j \leq y \leq y_{j+1}\}.$$

Then, at $t = 0$, we initialize the volume-of-fluid function in each computational cell as follows

$$F_{ij} = \frac{1}{\Delta x \Delta y}\int_{\Omega ij} H(\phi(x,y,0))dxdy.$$

In this case, $\Delta x = x_{i+1} - x_i$ and $\Delta y = y_{j+1} - y_j$, and $H(\phi)$ is the Heaviside function defined in (9). ϕ and F are evaluated at the cell centers so we have ϕ_{ij} and F_{ij}.

Both the level set equation and the volume-of-fluid equation are discretized using second order "strang splitting" (see Strang (1968)). The spatial operators are split, where one alternates between sweeping in the x direction,

$$\frac{F^* - F^n}{\Delta t} + \frac{u_{i+1/2,j}F^n_{i+1/2,j} - u_{i-1/2,j}F^n_{i-1/2,j}}{\Delta x} = F^*\frac{u_{i+1/2,j} - u_{i-1/2,j}}{\Delta x}$$

$$\frac{\phi^* - \phi^n}{\Delta t} + \frac{u_{i+1/2,j}\phi^n_{i+1/2,j} - u_{i-1/2,j}\phi^n_{i-1/2,j}}{\Delta x} = \phi^*\frac{u_{i+1/2,j} - u_{i-1/2,j}}{\Delta x},$$

and in the y direction,

$$\frac{F^{n+1} - F^*}{\Delta t} + \frac{v_{i,j+1/2}F^*_{i,j+1/2} - v_{i,j-1/2}F^*_{i,j-1/2}}{\Delta y} = F^*\frac{v_{i,j+1/2} - v_{i,j-1/2}}{\Delta y}$$

$$\frac{\phi^{n+1} - \phi^*}{\Delta t} + \frac{v_{i,j+1/2}\phi^*_{i,j+1/2} - v_{i,j-1/2}\phi^*_{i,j-1/2}}{\Delta y} = \phi^*\frac{v_{i,j+1/2} - v_{i,j-1/2}}{\Delta y}.$$

The volume-of-fluid fluxes, $F_{i+1/2,j}$, $F_{i,j+1/2}$, are calculated as the fraction of liquid fluid to the overall fluid that is advected across a given cell face during a time step. The level set fluxes, $\phi_{i+1/2,j}$ and $\phi_{i,j+1/2}$ are calculated by extrapolating the level set function in space and time to get a time-centered flux at given cell faces. Details are presented by Sussman and Puckett (2000).

3.2 Runge-Kutta/Crank-Nicolson projection method

Our numerical method for updating the momentum equations is based on the projection method proposed by Bell, Colella, and Glaz (1989). A general outline of the method can be given in terms of two sweeps:

Sweep 1:

$$\frac{\mathbf{u}^* - \mathbf{u}^n}{\Delta t} = F(\mathbf{u}^n) + G\left(\frac{\mathbf{u}^n + \mathbf{u}^*}{2}\right) - Gp^{n-1/2}$$
$$\frac{\mathbf{u}^{n+1,(0)} - \mathbf{u}^n}{\Delta t} = F(\mathbf{u}^n) + G\left(\frac{\mathbf{u}^n + \mathbf{u}^*}{2}\right) - Gp^{n+1/2,(0)} \quad (10)$$

Sweep 2:

$$\frac{\mathbf{u}^* - \mathbf{u}^n}{\Delta t} = F\left(\frac{\mathbf{u}^n + \mathbf{u}^{n+1,(0)}}{2}\right) + G\left(\frac{\mathbf{u}^n + \mathbf{u}^*}{2}\right) - Gp^{n+1/2,(0)}$$
$$\frac{\mathbf{u}^{n+1} - \mathbf{u}^n}{\Delta t} = F\left(\frac{\mathbf{u}^n + \mathbf{u}^{n+1,(0)}}{2}\right) + G\left(\frac{\mathbf{u}^n + \mathbf{u}^*}{2}\right) - Gp^{n+1/2} \quad (11)$$

$F(\mathbf{u})$ represents the discretization of the nonlinear advective terms, $G(\mathbf{u})$ represents the discretization of the viscosity terms, and Gp represents the pressure gradient term. The pressure update in (10) and (11) is cast as an elliptic equation for p and uses the continuity condition, $\nabla \cdot \mathbf{u} = 0$:

$$\nabla \cdot \frac{\nabla p}{\rho} = \nabla \cdot \mathbf{v}$$
$$\mathbf{u} = \mathbf{v} - \frac{\nabla p}{\rho}$$

3.3 Staggered grid discretization

The discrete velocity field is stored at cell face centers (MAC grid) and the pressure p, level set function ϕ, volume-of-fluid function F, viscous forces, nonlinear advection terms, and configuration tensor $\mathbf{A}$ are stored at cell centers. We store liquid and gas states separately. Our numerical discretization is designed so that our two-phase method is discretely equivalent to the second order method described by Sussman (2003) in the limit that the gas density approaches zero. In other words, the results of our computations are the same as if we had treated the gas pressure as spatially uniform.

An outline of our numerical algorithm during the first sweep of our Runge-Kutta/Crank-Nicolson time stepping procedure is given as the following sequence of steps:

1. Advance the location of the interface; update ϕ^{n+1} and F^{n+1}.

2. Calculate nonlinear advective terms using second order, Van-Leer limited slope calculation:

$$((\mathbf{u}\cdot\nabla)\mathbf{u})^n_{i,j} = \begin{cases} (\mathbf{u}_S \cdot \nabla)\mathbf{u}_S & \text{if } \phi \geq 0 \\ (\mathbf{u}_G \cdot \nabla)\mathbf{u}_G & \text{if } \phi < 0. \end{cases}$$

3. Update the configuration tensor $\mathbf{A}$. An important concern in the discretization of (7) is that $\mathbf{A}$ be maintained positive definite (Trebotich, Colella, and Miller (2005); Singh and Leal (1993)). The following steps are used to update $\mathbf{A}$:

   (a)

   $$\frac{\mathbf{A}^{adv} - \mathbf{A}^n}{\Delta t} + \left[\mathbf{u}\cdot\nabla\mathbf{A}\right]^n = 0$$

   A first-order upwind scheme is used for the term $[\mathbf{u}\cdot\nabla\mathbf{A}]^n$. The condition

   $$(u+v)\Delta t < \Delta x$$

   guarantees that if $\mathbf{A}^n$ is positive definite, then $\mathbf{A}^{adv}$ is also positive definite.

   (b) non-positive preserving update of $\mathbf{A}$,

   $$\frac{\mathbf{A}^{n+1} - \mathbf{A}^n}{\Delta t} = \left(\nabla\mathbf{u}\cdot\mathbf{A}\right)^n + \left(\mathbf{A}\cdot\nabla\mathbf{u}^T\right)^n - \frac{\mathbf{A}^{n+1}}{\lambda}$$

   (c) diagonally positive preserving update of $\mathbf{A}$, if $\left[\left(\nabla\mathbf{u}\cdot\mathbf{A}\right)^n + \left(\mathbf{A}\cdot\nabla\mathbf{u}^T\right)^n\right]_{ii} < 0$,

   $$\left[\frac{\mathbf{A}^{n+1} - \mathbf{A}^n}{\Delta t}\right]_{ii} = \left[\left(\left(\nabla\mathbf{u}\cdot\mathbf{A}\right)^n + \left(\mathbf{A}\cdot\nabla\mathbf{u}^T\right)^n\right)\frac{\mathbf{A}^{n+1}}{\mathbf{A}^n}\right]_{ii} - \left[\frac{\mathbf{A}^{n+1}}{\lambda}\right]_{ii}$$

4. Viscous solve,

$$\frac{\mathbf{u}^*_{i,j}-\mathbf{u}^n_{i,j}}{\Delta t} = -\left((\mathbf{u}\cdot\nabla)\mathbf{u}\right)^n_{i,j} - \left(\frac{\nabla p+\sigma\kappa\nabla H}{\rho}\right)^{n-1/2}_{i,j} + \left(\frac{1}{\rho}\nabla\cdot 2\eta_S\left(\frac{\mathbf{D}^n+\mathbf{D}^*}{2}\right)\right)_{i,j} + \left(\frac{1}{\rho}\nabla\cdot\frac{\eta_P\mathbf{A}}{\lambda}\right)^n_{i,j},$$

The viscosity (face centered) and density (cell centered here) as they appear above are discretized based on a finite-volume approach in which,

$$\tilde{\eta}_{S,i+1/2,j} = A_{i+1/2,j}\eta_S + (1-A_{i+1/2,j})\eta_G$$

$$\rho_{i,j} = F_{i,j}\rho_S + (1-F_{i,j})\rho_G.$$

In discretizing the viscoelastic force term, we replace $\frac{\eta_P\mathbf{A}}{\lambda}$ with,

$$\frac{\eta_P\mathbf{A}}{\lambda} = 2\eta_P\mathbf{D} - \eta_P\frac{\check{D}\mathbf{A}}{Dt},$$

where $\check{D}/Dt$ denotes the upper convected derivative (Bird, Armstrong, and O.Hassager (1987)). So that we now have

$$\frac{\mathbf{u}^*_{i,j}-\mathbf{u}^n_{i,j}}{\Delta t} = -\left((\mathbf{u}\cdot\nabla)\mathbf{u}\right)^n_{i,j} - \left(\frac{\nabla p+\sigma\kappa\nabla H}{\rho}\right)^{n-1/2}_{i,j} + \left(\frac{1}{\rho}\nabla\cdot 2(\tilde{\eta}_S+\tilde{\eta}_P)\left(\frac{\mathbf{D}^n+\mathbf{D}^*}{2}\right)\right)_{i,j} - \left(\nabla\cdot\frac{\tilde{\eta}_P\check{D}\mathbf{A}}{Dt}\right)_{i,j},$$

where

$$\frac{\check{D}\mathbf{A}}{Dt} = \frac{\mathbf{A}^{n+1}-\mathbf{A}^n}{\Delta t} - \left((\mathbf{u}\cdot\nabla)\mathbf{A}\right)^n + (\nabla\mathbf{u}\cdot\mathbf{A})^n + \left(\mathbf{A}\cdot\nabla\mathbf{u}^T\right)^n.$$

5. Interpolate advective force from cell centers to faces (liquid and gas advective terms interpolated separately),

$$\left[(\mathbf{u}\cdot\nabla)\mathbf{u}\right]_{i+1/2,j} = \frac{1}{2}\left[\left((\mathbf{u}\cdot\nabla)\mathbf{u}\right)_{i,j} + \left((\mathbf{u}\cdot\nabla)\mathbf{u}\right)_{i+1,j}\right]$$

6. Interpolate viscous force from cell centers to faces using a density-weighted average,

$$\left(\frac{1}{\rho}\nabla\cdot 2\tilde{\eta}_S\mathbf{D}\right)_{i+1/2,j} = \frac{1}{2}\frac{\left(\nabla\cdot 2\tilde{\eta}_S\mathbf{D}\right)_{i,j}}{\rho_{i,j}+\rho_{i+1,j}} + \frac{1}{2}\frac{\left(\nabla\cdot 2\tilde{\eta}_S\mathbf{D}\right)_{i+1,j}}{\rho_{i,j}+\rho_{i+1,j}}.$$

Density-weighted averaging is also used to interpolate the viscoelastic force from cell centers to faces.

7. Projection step.

   (a) For the liquid and gas separately,

$$\mathbf{u}^*_{i+1/2,j} = \mathbf{u}^n_{i+1/2,j} - \Delta t\left[(\mathbf{u}\cdot\nabla)\mathbf{u}\right]_{i+1/2,j} + \Delta t\left(\frac{1}{\rho}\nabla\cdot 2\tilde{\eta}_S\mathbf{D}\right)_{i+1/2,j} + \Delta t\left(\frac{1}{\rho}\nabla\cdot\frac{\tilde{\eta}_P\mathbf{A}}{\lambda}\right)_{i+1/2,j} - \Delta t\left(\frac{\sigma\kappa\nabla H}{\rho}\right)_{i+1/2,j}. \tag{12}$$

   (b)

$$\mathbf{u}^*_{i+1/2,j} = \begin{cases} (\mathbf{u}^*_{i+1/2,j})_S & \phi_{i,j}\geq 0 \text{ or } \phi_{i+1,j}\geq 0 \\ (\mathbf{u}^*_{i+1/2,j})_G & \text{otherwise.}\end{cases}$$

   (c)

$$\Delta t\nabla\cdot\frac{\nabla p^{n+1/2}}{\rho} = \nabla\cdot\mathbf{u}^*$$

$$\mathbf{u}^{n+1}_{i+1/2} = \mathbf{u}^*_{i+1/2} - \Delta t\frac{\nabla p^{n+1/2}}{\rho} \tag{13}$$

   Extrapolate $(\mathbf{u}^{n+1}_{i+1/2,j})_S$ where $\phi_{i,j}<0$ and $\phi_{i+1,j}<0$ (see Sussman (2003) for extrapolation details).

   (d)

$$\left(\frac{\nabla p-\sigma\kappa\nabla H}{\rho}\right)^{n+1/2}_{i,j} = \frac{\mathbf{u}^*_{i,j}-\mathbf{u}^{n+1}_{i,j}}{\Delta t} + \left(\frac{\nabla p+\sigma\kappa\nabla H}{\rho}\right)^{n-1/2}_{i,j}$$

As a remark, in the absence of viscous or viscoelastic forces, our two-phase numerical algorithm reduces to the second order single-phase numerical algorithm described by Sussman (2003) in the limit of zero gas density. In other words, for the problems described in this paper, the gas exerts primarily a normal pressure force on the liquid. Or to put it another way, the purpose of the gas is to take up volume. Our numerical method is consistent with this fact in that our numerical approach reduces to an approach in which the gas pressure is treated as spatially constant, and the liquid is incompressible. There are two important similarities between the two-phase approach presented here and the second order single-phase approach presented by Sussman (2003) in the limit of zero gas density. (1) The discretization of the surface tension force term (12), $\sigma\kappa\nabla H/\rho$ corresponds on the *discrete* level to the second order dirichlet boundary condition for surface tension that is described in Sussman (2003). (2) In this paper, we store the liquid velocity and gas velocity separately; the two velocity fields are distinguished by the liquid extrapolation step. The extrapolation step (just after (13)) is necessary in order to eliminate numerical diffusion in the liquid at the free surface. The extrapolation step used in this paper for two-fluids, has a corresponding role in the single-phase paper of Sussman (2003).

4 Results and Discussion

4.1 Axisymmetric Newtonian Bubble Shapes

In this section, we compute the steady state shapes of a gas bubble rising in a viscous Newtonian liquid. Grace, Wairegi, and Nguyen (1976) and, in a more detailed study, Bhaga and Weber (1981) systematically arranged the motion of bubbles freely rising in viscous Newtonian liquids. They showed that the Reynolds (Re), Eötvös (Eo) and Morton (Mo) numbers were essential for describing a rising bubble (drop) or falling drop motion because the shape and terminal velocity of a bubble or drop are determined by these three dimensionless numbers. As in Bhaga and Weber (1981), Hnat and Buckmaster (1976) and Grace, Wairegi, and Nguyen (1976), we will present our computational results in terms of these dimensionless groups. The Reynolds number Re, the Eötvös number Eo, and the Morton number Mo are defined as follows

$$\mathrm{Re} = \frac{\rho_S L U}{\eta_S} \qquad \mathrm{Eo} = \frac{\rho_S L^2 g}{\sigma} \qquad \mathrm{Mo} = \frac{g\eta_S^4}{\rho_S \sigma^3}. \tag{14}$$

ρ_S is the solvent density, L is the bubble diameter, U is a characteristic velocity, η_S is the solvent viscosity, σ is the surface tension, and g is the acceleration of gravity.

Another set of useful dimensionless numbers, although not independent of those in (14), are the Weber number We, the Froude number Fr, and the drag coefficient C_D :

$$\mathrm{We} = \frac{\rho_S L U^2}{\sigma} \qquad \mathrm{Fr} = \frac{U^2}{gL} \qquad C_D = \frac{4\rho_S g L^2}{3\eta_S U}.$$

We shall compare our computational results with the experimental results found in Bhaga and Weber (1981) and Hnat and Buckmaster (1976) and computational results in Ryskin and Leal (1984).

It should be noted that in our computations the rise velocity U of the bubble is not known *a priori*; a reference bubble velocity is chosen so the relevant dimensionless parameters coincide with those of the experiments performed by Bhaga and Weber (1981) and Hnat and Buckmaster (1976).

Figure 1 is an oblate ellipsoidal cap bubble found by Bhaga and Weber (1981). The left part of the image in Figure 1 corresponds to bubble (d) of figure 2 in their study, where Eo = 243, Mo = 266, and Re = 7.77. The right side of the image is our computational result which shows an indentation at the base of the bubble, in agreement with experimental observations.

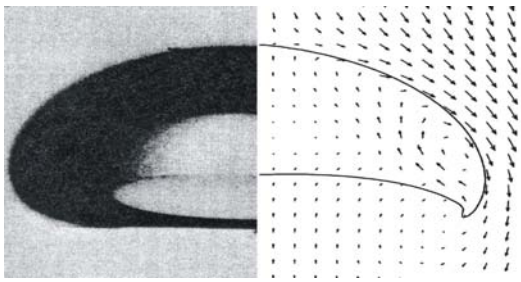

Figure 1 : Comparison of our numerical results with experimental results found in Bhaga and Weber (1981) where Eo = 243, Mo = 266, and Re = 7.77.

The work of Hnat and Buckmaster (1976) studies the structure of spherical cap bubbles and skirt formation in mineral oil (high liquid-gas density ratio and viscosity

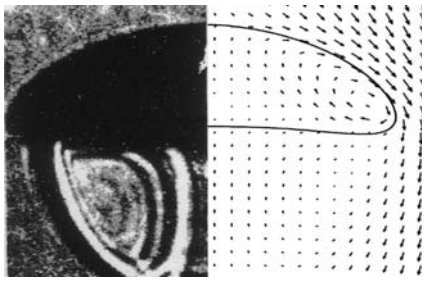

Figure 2 : Comparison of our numerical results with experimental results found in Hnat and Buckmaster (1976) where Re $= 9.8$, Mo $= 0.065$, and $C = 4.95$.

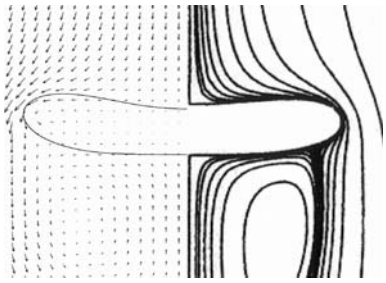

Figure 3 : Comparison of our numerical results with computational results found in Ryskin and Leal (1984) where Re $= 100$ and We $= 10$.

ratio). The photograph in the left side of Figure 2 corresponds to the spherical cap bubble Figure 1(a) found in their study. The right side of this figure corresponds to our computational results. From Figure 2 we see that our computational results closely agree with their experimental findings. In this case, the relevant parameters are Re $= 9.8$, Mo $= 0.065$, and $C = 4.95$, where

$$C = \frac{r}{(\nu^2/g)^{1/3}}$$

is a nondimensional parameter, r is the effective bubble radius, ν is the kinematic viscosity, and g is the acceleration of gravity.

In Ryskin and Leal (1984), they consider the numerical solution of buoyancy-driven motion of a gas bubble in a quiescent fluid using a boundary-fitted finite difference method. To compare with their numerical results, we present our computations in terms of the Reynolds number Re and Weber number We. Figure 3 corresponds to Re $= 100$ and We $= 10$; the same figure can be found in their work. As with the experimental results, we find that a comparison of our numerical findings to their computational results show reasonable agreement.

4.2 Gas Bubble Bursting at a Free Surface

In this section we consider the problem of a gas bubble bursting at the free surface of a liquid. A similar problem has been studies computationally by Boulton-Stone and Blake (1993) and Sussman and Smereka (1997). In our computations, we illustrate the differences between a gas bubble bursting from a Newtonian fluid versus a gas bubble bursting from a viscoelastic fluid. The setup of the problem is as follows. We initialize a spherical gas bubble just below the surface of the liquid. Strong surface tension forces give rise to a vertical liquid jet.

In both cases, the Newtonian as well as the viscoelastic case, we have a liquid-gas density ratio of 1000:1 and a liquid-gas viscosity ratio of 100:1. To make comparisons with previous similar gas-bursting computations (Sussman and Smereka (1997)), we assume a characteristic velocity of $U = 26$ cm/s. This is done to set Re $= 100$. We also use a characteristic length scale of $l = 1.1$ cm (radius of bubble), and a fictitious solvent viscosity of $\eta_S = 0.286$ g/(cm·s). This gives the following dimensionless values,

$$\mathrm{Re} = \frac{\rho_S l U}{\eta_S} = 100,$$

$$\mathrm{Fr} = \frac{U^2}{gl} = 0.64,$$

$$\mathrm{We} = \frac{\rho_S l U^2}{\sigma} = 10.$$

For the non-newtonian case, we assume the same characteristic velocity $U = 26$ cm/s, and a characteristic length scale of $l = 1.1$ cm (radius of bubble), but we assume that the fictitious liquid viscosity is zero ($\eta_S = 0$), and the fictitious polymeric viscosity satisfies $\eta_P = 0.005$. Also, we assume that L as it appears in (8) satisfies $L = 10$ and the Deborah number,

$$\mathrm{De} = \frac{U\lambda}{l},$$

is De=236. As expected, the added effects of viscoelasticity drastically change the dynamics of the bubble-jet system. We perform our calculations in a domain $\Omega = \Omega_S \cup \Omega_G = \{(r,z) \,|\, 0 \le r \le 3, 0 \le z \le 12\}$ with a 16×64 grid with one level of Adaptive Mesh Refinement (AMR)

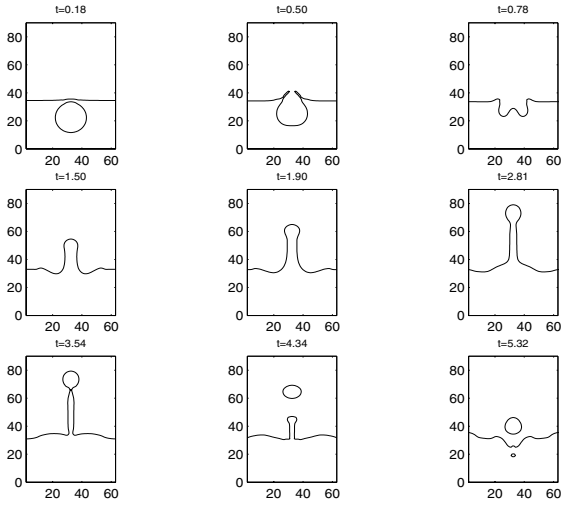

Figure 4 : Gas bubble bursting at a free surface of a Newtonian fluid.

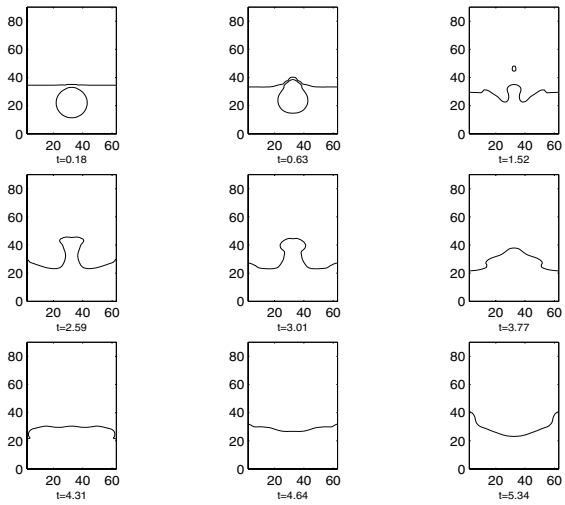

Figure 5 : Gas bubble bursting at a free surface of a viscoelastic fluid.

(see Sussman, Almgren, Bell, Collela, Howell, and Welcome (1999) and Sussman (2005) for AMR information). As our submerged gas bubble breaks through the surface, the resulting large surface tension forces produced ultimately result in the ejection of a liquid jet. In the absence of viscoelastic effects, the Newtonian liquid jet is ejected upwards more forcefully and eventually pinches off. We remark that the level set formulation allows the computation to continue well after the liquid jet breaks. A drop is formed as a result of the pinch-off and, as this drop impinges on the liquid on its way back, it entrains a small gas bubble just below the surface (see Figure 4).

On the other hand, using the same initial conditions, the viscoelastic fluid attenuates the liquid jet dynamics. As in the Newtonian fluid, in this case we also observe the formation of a liquid jet after the bubble breaks the surface. However, the jet profile is wider and elastic effects prevent it from extending as high as the Newtonian jet (see Figure 5). The spring-like viscosity of the solvent force the jet to recoil more abruptly as the fluid attempts to reach an equilibrium state. We also notice that in this case the viscoelastic effects render the jet more resistant to pinch off.

We remark that our results demonstrate that we can obtain comparable results as a body-fitted approach, with the additional feature of calculating multiphase flows with "complex" geometry.

4.3 Steady Viscoelastic Bubble Rise Motion

In this section we study the steady state shape of a gas bubble rising in a viscoelastic fluid. As a reference, we refer the reader to Noh, Kang, and Leal (1993). We compute the steady deformation of an axisymmetric gas bubble of radius r rising with velocity U in a viscoelastic (polymeric) solution of density ρ_S. The solvent is a polymeric solution with viscosity η_S. We will also assume there is a uniform surface bubble tension σ. The density ratio and viscosity ratio in our computations are taken to be 1000:1 and 100:1 respectively.

The governing equations are given by (4). Using a characteristic velocity $U = 0.187$ m/s, and a characteristic length scale (bubble diameter) $l = 20$ mm, we have,

$$\mathrm{Re} = \frac{\rho_S l U}{\eta_S} = 3.4,$$

$$\mathrm{Fr} = \frac{U^2}{gl} = 0.178,$$

$$\mathrm{We} = \frac{\rho_S l U^2}{\sigma} = 14,$$

and

$$\mathrm{Ca} = \frac{\mathrm{We}}{\mathrm{Re}} = 4.114.$$

In all of our examples, $\eta_P = c\eta_S$ where $c = 0.1$. Figures 6-8 show the steady state shape of a gas bubble rising in various polymeric solutions. We examine the resulting bubble geometry as we vary L (8) and the Deborah number,

$$\mathrm{De} = \frac{U\lambda}{l}.$$

We notice in Figures 6 and 7 the bubble shape exhibits the well-known trailing cusp, characteristic of gas bubbles rising in viscoelastic fluids.

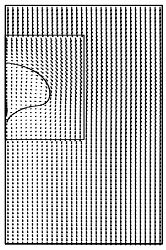

Figure 6 : Computational results for $L = 10$, $\mathrm{De} = 10$ and $c = 0.1$.

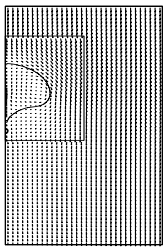

Figure 7 : Computational results for $L = 10$, $\mathrm{De} = 5$, and $c = 0.1$.

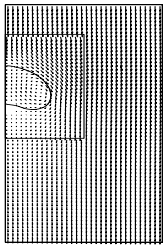

Figure 8 : Computational results for $L = 5$, $\mathrm{De} = 10$, and $c = 0.1$.

5 Conclusions

We have presented a coupled level set method and volume-of-fluid method for computing axisymmetric bubble motion in Newtonian and viscoelastic fluids. Using this method, our computations demonstrated reasonable agreement with previous computational results as well as benchmark experimental results. In addition, we showed that using our method we can easily continue our computation even in the presence of complex topological changes, such as jet pinch-off and bubble entrainment. Moreover, the addition of AMR allows us to investigate finer properties of liquid-gas dynamics in both Newtonian and viscoelastic fluids.

Acknowledgement: Research supported in part by NSF and JSPS.

References

Bechtel, S.; Forest, G.; Wang, Q.; Zhou, H. (1998): Free surface viscoelastic and liquid crystalline polymer fibers and jets. In Siginer, D.; DeKeee, D.; Chabra, R.(Eds): *Advances in Non-Newtonian Flows and Rheology*. Elsevier Science.

Bell, J. B.; Colella, P.; Glaz, H. M. (1989): A second-order projection method for the incompressible Navier-Stokes equations. *J. Comput. Phys.*, vol. 85, pp. 257–283.

Bhaga, D.; Weber, M. (1981): Bubbles in viscous liquids: Shapes, wakes, and velocities. *J. Fluid Mech.*, vol. 105, pp. 61–85.

Bird, R. B.; Armstrong, R.; O.Hassager (1987): *Dynamics of Polymeric Fluids, 2nd ed.* John Wiley & Sons.

Boulton-Stone, J.; Blake, J. (1993): Gas bubbles bursting at a free surface. *J. Fluid Mech.*, vol. 254, pp. 437–466.

Brackbill, J. U.; Kothe, D. B.; Zemach, C. (1992): A continuum method for modeling surface tension. *J. Comput. Phys.*, vol. 100, pp. 335–353.

Chilcott, M.; Rallison, J. (1988): Creeping flow of dilute polymer solutions past cylinders and spheres. *J. Non-newtonian fluid mech.*, vol. 29, pp. 381.

Esmaeeli, A. (2005): Phase distribution of bubbly flows under terrestrial and microgravity conditions. *FDMP*, vol. 1, no. 1, pp. 63–80.

Goktekin, T.; Bargteil, A.; O'Brien, J. (2004): A method for animating viscoelastic fluids. *ACM Transactions on Graphics (TOG)*, vol. 23(3), pp. 463–468.

Grace, J.; Wairegi, T.; Nguyen, T. (1976): Shapes and velocities of single drops and bubbles moving freely through immiscible liquids. *Trans. Instn. Chem. Engrs.*, vol. 54, pp. 167–173.

Hnat, J.; Buckmaster, J. (1976): Spherical cap bubbles and skirt formation. *Phys. Fluids*, vol. 19, no. 2, pp. 182–194.

Jansseune, T.; Mewis, J.; Moldenaers, P.; Minale, M.; Maffettone, P. (2000): Rheology and rheological morphology determination in immiscible two-phase polymer model blends. *J. Non-Newtonian Fluid Mech.*, vol. 93, pp. 153–165.

Kang, M.; Fedkiw, R.; Liu, X.-D. (2000): A boundary condition capturing method for multiphase incompressible flow. *J. Sci. Comput.*, vol. 15, pp. 323–360.

Marten, K.; Shariff, K.; Psarakos, S.; White, D. (1996): Ring bubbles of dolphins. *Sci. Amer.*, vol. 275, pp. 83–87.

Migler, K.; Son, Y.; Qiao, F.; Flynn, K. (2002): Extensional deformation, cohesive failure, and boundary conditions during sharkskin melt fracture. *J. Rheol.*, vol. 46, no. 2, pp. 383–400.

Nithi-Uthai, N.; Manas-Zloczower, I. (2003): Numerical simulation of sharkskin phenomena in polymer melts. *Applied Rheology*, vol. 13, pp. 79–86.

Noh, D.; Kang, I.; Leal, L. (1993): Numerical solutions for the deformation of a bubble rising in dilute polymeric fluids. *Phys. Fluids A*, vol. 5, no. 6, pp. 1315–1332.

Ohta, M.; Imura, T.; Yoshida, Y.; Sussman, M. (2005): A computational study of the effect of initial bubble conditions on the motion of a gas bubble rising in viscous fluids. *Int. J. Multiphase Flow*, vol. 31, pp. 223–237.

Pillapakkam, S.; Singh, P. (2001): A level set method for computing solutions to viscoelastic two-phase flow. *Journal of Computational Physics*, vol. 174, pp. 552–578.

Rudman, M. (1998): A volume-tracking method for incompressible multifluid flows with large density variations. *International J. for numerical methods in fluids*, vol. 28, pp. 357–378.

Ryskin, G.; Leal, L. (1984): Numerical solution of free-boundary problems in fluid mechanics. part 2. buoyancy-driven motion of a gas bubble through a quiescent liquid. *J. Fluid Mech.*, vol. 148, pp. 19–35.

Sethian, J. (1999): *Level Set Methods and Fast Marching Methods: Evolving Interfaces in Computational Geometry, Fluid Mechanics, Computer Vision, and Materials Science*. Cambridge University Press, 2nd edition.

Singh, P.; Leal, L. (1993): Finite-element simulation of the start-up problem for a viscoelastic fluid in an eccentric rotating cylinder geometry using a third-order upwind scheme. *Theoret. Comput. Fluid Dynamics*, vol. 5, pp. 107–137.

Strang, G. (1968): On the construction and comparison of difference schemes. *SIAM J. Numer. Anal.*, vol. 5, pp. 506.

Sussman, M. (2003): A second order coupled level set and volume-of-fluid method for computing growth and collapse of vapor bubbles. *J. Comput. Phys.*, vol. 187, pp. 110–136.

Sussman, M. (2005): A parallelized, adaptive algorithm for multiphase flows in general geometries. *International Journal of Computers and Structures*, vol. 83, pp. 435–444.

Sussman, M.; Almgren, A.; Bell, J.; Collela, P.; Howell, L.; Welcome, M. (1999): An adaptive level set approach for incompressible two-phase flows. *J. Comput. Phys.*, vol. 148, pp. 81–124.

Sussman, M.; Hussaini, M.; Smith, K.; Zhi-Wei, R.; Mihalef, V. (2004): A second order adaptive sharp interface method for incompressible multiphase flow. In *Proceedings of the 3rd international conference on Computational Fluid Dynamics*, Toronto, Canada. to appear.

Sussman, M.; Puckett, E. (2000): A coupled level set and volume-of-fluid method for computing 3d and axisymmetric incompressible two-phase flows. *J. Comput. Phys.*, vol. 162, pp. 301–337.

Sussman, M.; Smereka, P. (1997): Axisymmetric free boundary problems. *J. Fluid Mech.*, vol. 341, pp. 269–294.

Sussman, M.; Smereka, P.; Osher, S. (1994): A level set approach for computing solutions to incompressible two-phase flow. *J. Comput. Phys.*, vol. 114, pp. 146–159.

Trebotich, D.; Colella, P.; Miller, G. (2005): A stable and convergent scheme for viscoelastic flow in contraction channels. *J. Comput. Phys.*, vol. 205, pp. 315–342.

Unverdi, S. O.; Tryggvason, G. (1992): A front-tracking method for viscous, incompressible, multi-fluid flows. *J. Comput. Phys.*, vol. 100, pp. 25–37.

Venet, C.; Vergnes, B. (2000): Stress distribution around capillary die exit: an interpretation of the onset of sharkskin defect. *J. Non-Newtonian Fluid Mechanics*, vol. 93, pp. 117–132.